

# Nanoscale

Accepted Manuscript



This is an *Accepted Manuscript*, which has been through the Royal Society of Chemistry peer review process and has been accepted for publication.

*Accepted Manuscripts* are published online shortly after acceptance, before technical editing, formatting and proof reading. Using this free service, authors can make their results available to the community, in citable form, before we publish the edited article. We will replace this *Accepted Manuscript* with the edited and formatted *Advance Article* as soon as it is available.

You can find more information about *Accepted Manuscripts* in the [Information for Authors](#).

Please note that technical editing may introduce minor changes to the text and/or graphics, which may alter content. The journal's standard [Terms & Conditions](#) and the [Ethical guidelines](#) still apply. In no event shall the Royal Society of Chemistry be held responsible for any errors or omissions in this *Accepted Manuscript* or any consequences arising from the use of any information it contains.

## Grating-Structured Metallic Microsprings

Tao Huang,<sup>ab</sup> Zhaoqian Liu,<sup>ab</sup> Gaoshan Huang,<sup>b</sup> Ran Liu,<sup>a,\*</sup> Yongfeng Mei<sup>b,\*</sup>

Cite this: DOI: 10.1039/x0xx00000x

Received 00th January 2014,  
3 Accepted 00th January 2014

DOI: 10.1039/x0xx00000x

www.rsc.org/

6

9 We fabricate grating-structured metallic microsprings with well-defined helical angles  
and diameters, which are self-rolled from strained nanomembranes patterned with  
12 gratings. The grating structures on the metal membrane, replicated from the imprinted  
polymer layer beneath, give rise to the controlled rolling direction after selectively  
etching of the underlying sacrificial layer. The rolling direction of grating-structured  
thin metal film is always perpendicular to the long side edge of gratings, offering a good  
15 way to roll up strained strips into well controlled three-dimensional (3D) microsprings  
simply by altering the dimension and orientation of the structured strips. The  
mechanical elasticity of these grating-structured metallic microsprings is verified for the  
18 potential application as a flow rate sensor. Our work may stimulate rigorous synthesis of  
highly functional and complex 3D helical micro and nanostructures, and hint a broad  
range of applications such as environmental sensors, micro-/nanoscale robots, and  
21 metamaterials, etc.

### 1 Introduction

24 Design and synthesis of a rich variety of two or three-  
dimensional structures with some intriguing shapes like  
tubes,<sup>1</sup> rods,<sup>2</sup> helices,<sup>3</sup> and cones<sup>4</sup> at micro- and nanoscale  
have triggered a lot of research excitement for decades.  
27 These unique micro-/nanostructures display fascinating  
optical, mechanical, electrical, and catalytic properties,<sup>5-9</sup>  
which basically accelerate their applications in fields such as  
30 energy harvesting,<sup>10</sup> bio-sensing,<sup>11</sup> optoelectronics,<sup>12</sup> and  
integrated circuits.<sup>13</sup> Three-dimensional micro-/nano-springs  
with tunable chirality and periodicity, emerging from these  
33 aforesaid structures, are envisioned an irreplaceable place in  
the miniature devices. To date, a number of materials have  
been exploited to synthesize various kinds of micro-/nano-  
36 springs or helical structures at different ordered dimensions  
for predictable utility, such as carbon nanocoils,<sup>14</sup> zinc oxide  
nanosprings,<sup>15</sup> InGaAs/GaAs nanohelices,<sup>16</sup> and Si spirals.<sup>17</sup>  
39 They have been found with benefits for the potential  
applications of electromechanical sensors and actuators,<sup>18</sup>  
bioengineering,<sup>19</sup> microrobots,<sup>20</sup> and electromagnetic wave  
42 absorbers.<sup>21</sup>

Though the complex structure of micro-/nano-springs  
endows themselves unique characteristics, the fabrication  
45 methods are inevitably limited by the traditional planar  
processes, even with the state of art techniques in recent  
days. Two general approaches, namely 'bottom-up' and  
48 'top-down', which are also called template-assisted and  
template-free methods, are simultaneously and separately

proposed to address this challenge. Typical 'bottom-up'  
51 examples, including chemical vapor deposition (CVD),<sup>15</sup>  
glancing angle deposition (GLAD),<sup>22</sup> and template  
method,<sup>23-25</sup> are experimentally proved to be less  
54 controllable and lower uniform for desired applications.  
Two alternative 'top-down' methods: Focused ion beam  
(FIB)<sup>26</sup> and laser direct writing (DLW)<sup>19</sup> exhibit highly  
57 accurate topology control, but commonly suffer from the  
drawbacks of high cost of instrument and time consumption.  
Recently, a convenient and robust methodology, namely  
60 rolled-up technology, opens new fabrication paths for micro-  
/nano-springs with high accuracy and good controllability by  
employing both 'bottom-up' and 'top-down' approaches.<sup>27</sup>  
63 Upon the release of internal strain after the etching of the  
underlying sacrificial layer, the patterned ribbons  
comprising of single material or different material  
66 combination will roll up into tubes or springs depending on  
the orientation of the strips with respect to the preferential  
rolling direction where the released films prefer to bend up.  
69 Generally, the preferential rolling direction can be generated  
in the films through technically designing and introducing  
anisotropic properties into the pre-rolling material layers  
72 such as the anisotropic Young's modulus on GaAs or Si  
substrate,<sup>16,28</sup> anisotropic sacrificial's etching behavior,<sup>29</sup>  
elastically isotropic film with geometrical anisotropy (high  
75 aspect ratio),<sup>30</sup> and glanced angle deposited (GLD)  
anisotropic metal film,<sup>31,32</sup> to name but a few. A case in  
point is that the well-controlled superelastic metal

microsprings,<sup>31</sup> fabricated by introducing Young's modulus anisotropy to the strained metal films during the glancing angle deposition (GLD) process, inherently possess a wide range of designed helical angles from 20° to 70° without any additional treatments compared to other work.<sup>28</sup>

So far, most approaches that can define and control the rolling direction as well as the position of as-fabricated micro-/nano-structures in strained engineering have been involved with lithographically defined etching window,<sup>29,33-35</sup> shadow effect induced by GLD,<sup>36</sup> and geometry effect.<sup>37</sup> Unlike the previous approaches to determine the preferential rolling direction *via* anisotropic geometry effect,<sup>37,38</sup> a novel strategy was recently put forward to manipulate the rolling behavior by simply introducing periodic wrinkles to initial rectangular nanomembranes.<sup>39</sup> These wrinkled nanomembranes preferred to bend up from the flat edge and the rolling direction was practically perpendicular to the long side edge of the wrinkles because bending from the wrinkled edge costs large additional energy to flatten the wrinkled film. As theoretically predicted, this effect can be maintained and enhanced by altering wrinkles' parameters such as the amplitude and the wavelength. Taking advantage of this robust and predictable control over the rolling direction, we thereafter demonstrate a reproducible route to fabricate the grating-structured metallic microsprings rolling from imprinted sacrificial layer with grating structures which play a deterministic role in deciding the rolling direction. The mechanical performance in flow rate sensing of the grating-structured metallic microsprings have been tested and analyzed. It can be anticipated that such novel approach to synthesize these fine textured metallic microsprings may broaden the way to fabricate highly functionalized and complex 3D structures in a controlled and parallel manner and make them potential candidates for applications in miniature electromechanical devices and metamaterials.

## 2 Experimental section

### 2.1 Fabrication of grating-structured microsprings

Silicon grating moulds of different period for nanoimprint lithography (NIL) were fabricated by the combination of laser interference lithography (LIL) and reactive ion etching (RIE). The moulds were cut into pieces of a square area of about 1 cm × 1 cm. Both the moulds and Si substrates were cleaned by ultrasonication in piranha solution (98%  $H_2SO_4$  : 30%  $H_2O_2$  = 3 : 1 at  $T = 90^\circ C$ ) and acetone for 10 min respectively, then rinsed abundantly with deionized water (DIW) and blown dry with  $N_2$  gas flow. A ~200 nm thin layer of PMMA was spin coated onto substrate and soft baked at  $T = 180^\circ C$  for 10 min. Nanoimprinting with moulds facing against the PMMA layer was performed at  $T = 180^\circ C$ , *i.e.* about 75 °C above its glass transition temperature ( $T_g = 105^\circ C$ ), under an imprint pressure of about 25 MPa.<sup>40</sup> After demolding, the grating structures

were transferred from the mould to the PMMA layer. Sequentially, a step between the PMMA layer and the substrate was created by the means discussed in previous work.<sup>31</sup> A shadow mask with fine designed rectangular apertures was covered closely onto the surface of the PMMA layer, and Ti films were deposited and patterned through the rectangles at a vacuum about  $2 \times 10^{-4}$  Pa *via* electron beam evaporation. Once immersed in acetone, the rectangular Ti nanomembranes were released and rolled up into microsprings by selectively underetching the PMMA layer,<sup>31</sup> and meanwhile the grating structures were precisely transferred to microsprings' walls. The as-fabricated grating-structured metallic microsprings were then dried in supercritical point drier (Leica CPD030) followed by the characterization of optical microscope (Olympus BX51) and scanning electron microscope (PHILIPS XL30 FEG).

### 2.2 Characterization of flow rate sensing

By placing this sensing system into glass conduit with a rectangular cross section of 2 cm × 4 cm, the whole part of the grating-structured microspring was floating in the fluid with one end fixed on Si substrate. The images of grating-structured microsprings at different fluid rate were recorded and collected by optical microscope (Olympus BX51) connected with a high speed camera.

## 3 Results and discussion

### 3.1 Fabrication of grating-structured metallic microsprings

Fig. 1a schematically illustrates the fabrication process of the grating-structured metallic microsprings combining thermal imprinting and rolling up. It should be noted that the spin-coated PMMA layer (as shown in panel I of Fig. 1a) serves as both the thermal resist in the NIL process and the sacrificial layer in the self-rolling, strongly suggesting that these two techniques are indeed compatible in our present experiment. The grating structures were initially introduced on the PMMA layer by nanoimprinting process as shown in panel II of Fig. 1a. It's worth noting that to guarantee a complete pattern transfer and simultaneously avert the metal deposition onto the bare grooves (*i.e.* exposed substrate between the grating lines) induced by direct contact between the mould and the substrate, a proper imprint pressure should be carefully adjusted. Moreover, opposite to the case of a general lift-off process,<sup>41</sup> the imprinting-mediated tapered profile of gratings (as schematically shown in Fig. S5 (a), ESI†) is rather suitable for depositing continuous thin metal film from the top to the bottom of gratings, which is essential for the following formation of the rolled-up grating-structured microsprings. Fig. 1b shows the SEM image of the imprinted grating structures with a period of ~3.4 μm on the PMMA layer (see the enlarged image in the inset). In

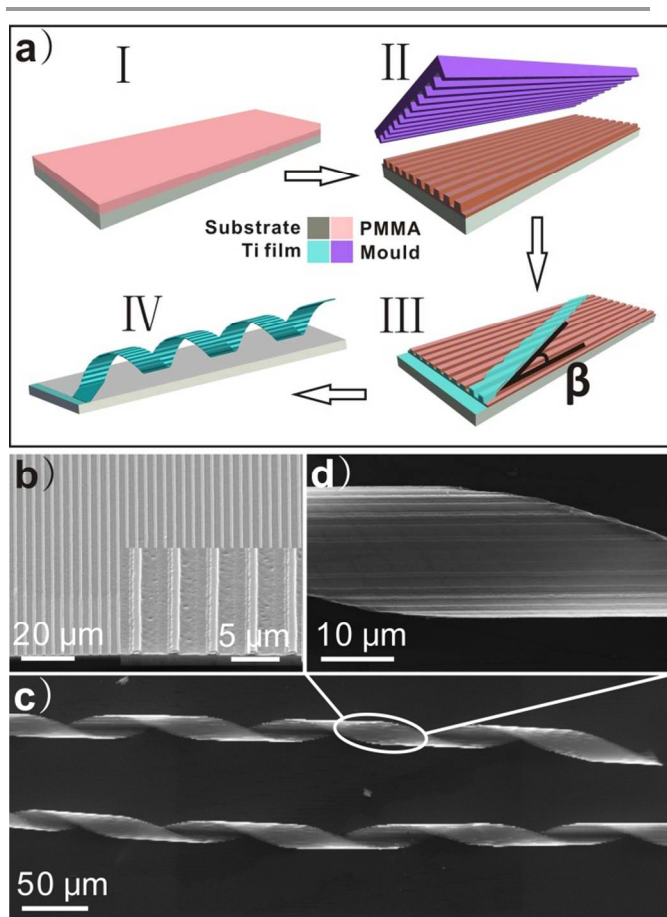


Fig. 1 (a) A basic process flow of fabricating the grating-structured metallic microsprings. (b) SEM image of typical imprinted grating structures on PMMA. Inset shows the gratings with a period of  $\sim 3.4 \mu\text{m}$  at higher magnification. (c) SEM image of the grating-structured metallic microsprings. (d) Close-up SEM image of a part of the grating-structured microspring in (c).

order to form microsprings, it's of crucial importance to make the long side of the deposited rectangular metal strips deviate from the direction of the long side of gratings. (This direction is proved to be perpendicular to the preferred rolling direction in our later discussion.) For the purpose of immobilizing microsprings on the substrate, a step between the substrate and the PMMA layer was necessary for the direct attachment of metal films on the substrate after deposition and thus preventing the complete release of the films after the PMMA removal. We might notice that the deposited metal nanomembranes (excluding the part on the top of the bared substrate for spring immobilization) were patterned into rectangles with a grating-structured topology transferred from the imprinted PMMA layer and a misaligned angle  $\beta$  with respect to the gratings as depicted in panel III of Fig. 1a. After the gradual removal of the PMMA layer (*i.e.* the sacrificial layer) synchronized with the release of the upper metal strips in acetone, the grating-structured metallic microsprings with one end fixed on the substrate (see panel IV of Fig. 1a) will get into shape in the fashionable manner, namely self-rolling. An SEM image of

typical as-fabricated grating-structured metallic microsprings was shown in Fig. 1c. The close-up SEM image in Fig. 1d reveals that the grating structures were successfully transferred from the PMMA layer to the walls of the microsprings. It was experimentally found that the etching rate of the sacrificial layer became much slower compared to our previous work,<sup>31</sup> which can be attributed to the low solubility of the sacrificial layer in acetone triggered by the cross-linking reaction of PMMA molecules occurring at high temperature during nanoimprinting.<sup>42</sup> The slower etching rate in this case efficiently suppressed the violent interaction from the solution and bubbles or even a film peeling-off case<sup>30</sup>, conducting to the positioning and immobilizing of microsprings.

### 3.2 Verification of preferential rolling direction

To study how the gratings influence the rolling direction of the strained rectangular nanomembranes, we have contrastively performed proving experiments at three different scenarios depicted in Fig. 2a. Two shadow masks with different aspect ratios were used: One has an array of high aspect-ratio rectangles with dimension of  $80 \mu\text{m} \times 500 \mu\text{m}$ , the other with dimension of  $20 \mu\text{m} \times 600 \mu\text{m}$ . The rectangular strips replicated from the first mask were deposited onto both the un-imprinted area (panel I of Fig. 2a) and the imprinted area (panel II of Fig. 2a) on a same substrate at the orientation of the long side of rectangles perpendicular to the long side of grating structures. The second mask was covered solely onto the imprinted area with the rectangles deviating off the gratings to a certain degree (see panel III of Fig. 2a). As illuminated in the right panel of Fig. 2a, all the metal nanomembranes rolled up from their long sides in panel I' whereas those rolled up from their short sides in panel II' and formed the grating-structured tubes without exception. And the misaligned rectangles (see panel III of Fig. 2a) rolled up into microsprings in panel III'. As experimentally presented in Fig. 2b,

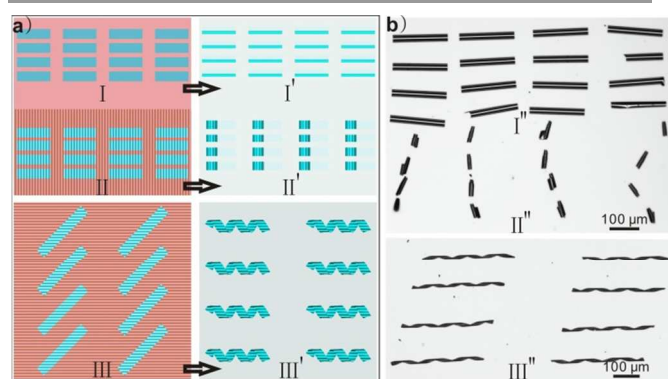


Fig. 2 (a) Schematic drawings illustrating three different cases before (left panel) and after (right panel) self-rolling to verify the exact rolling direction on the imprinted area. (b) Corresponding experimental observation: (I'') A  $4 \times 4$  array of long-side rolling tubes on the un-imprinted area; (II'') a  $4 \times 4$  array of short-side rolling grating-structured tubes; (III'') a  $2 \times 4$  array of grating-structured microsprings.

that the long-side rolling is preferred in this typical length to width ratio ( $\sim 6 : 1$ ) of the rectangles in the present experiment (see panel I'') and this rolling preference continues for a higher aspect ratio due to the geometry effect.<sup>37</sup> In contrast, the strips deposited on the grating structures showed a different rolling behavior, *i.e.* the rolling occurred from the short side (see panel II''). And no rolling from the long-side was observed after varying aspect ratios from 2 to 10 with a constant width of the strips (see Fig. S1, ESI†), agreeing well with the previous work<sup>39</sup> which has already proved that the rolling from the flat side is favorable in this regime. Herein, similar to the wrinkle mediated rolling process, this rolling behavior can be explained by the fact that the long side rolling of rectangles suffers from an elastic energy barrier required to flatten the grating structures. Given that no external force is engaged,<sup>43</sup> the elastic energy barrier adequately restrains the rolling tendency from the long side of rectangles since the self-rolling is basically an energy release or energy minimization process. Consequently, to minimize the elasticity energy of the membranes as much as possible, the rolling kinetically favors the direction perpendicular to the gratings, which is accordingly defined as the preferential rolling direction. On the other hand, a  $4 \times 2$  array of the grating-structured microsprings aligning themselves along the direction of the gratings in panel III'' were fabricated at the condition that the dimension of the rectangles belongs to the geometric regime for tube formation.<sup>30</sup> This also persuasively indicates that anisotropy property has been introduced to the metal film by remodeling the topology of the sacrificial layer before evaporation, because spring or coil can hardly be formed by self-rolling an isotropic nanomembrane at a tube-formation regime.<sup>30</sup>

### 3.3 Arbitrary helical angle design

Strained rectangular nanomembranes with anisotropic elastic properties have been engineered by introducing the imprinted gratings, yielding a preferential rolling direction perpendicular to the gratings. In the following, we have investigated whether the microsprings in different geometrical shapes could be defined and fabricated *via* misaligning the initial rectangular nanomembranes. In analogy to our previous work,<sup>31</sup> experiments were carried out in an expectation to get microsprings with arbitrary helical angles and further verify the preferential rolling direction perpendicular to the gratings. By simply varying the misaligned angle of the rectangles relative to the gratings (gratings period  $\lambda = \sim 3.4 \mu\text{m}$ ), which is denoted as  $\beta$  in both panel III of Fig. 1a and inset of Fig. 3b, microsprings with different geometries can take shape after selectively undercutting the PMMA layer. On the basis of the empirical relationship for spring geometry, we have:

$$\pi D \cdot \tan \alpha = p \quad (1)$$

where  $D$  is the diameter,  $p$  is the pitch.<sup>28</sup> The helical angle  $\alpha$  can thus be obtained by substituting the values of  $D$  and  $p$

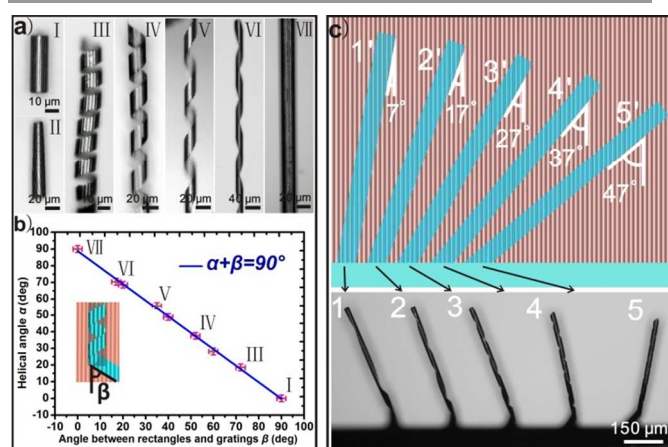


Fig. 3 (a) Optical images of the grating-structured metallic microsprings with a helical angle of  $18^\circ$  (III),  $38^\circ$  (IV),  $56^\circ$  (V), and  $70^\circ$  (VI); the grating-structured microtubes (I and VII); and the grating-structured microscrew (II). (Detailed geometry parameters are summarized in Table S1, ESI†.) (b) 2D plot of the calculated helical angle ( $\alpha$ ) as a function of the angle between rectangles and gratings ( $\beta$ ). The function solid line of  $\alpha + \beta = 90^\circ$  fits the experimental data. Inset schematically shows the configuration of the as-fabricated microspring and the residue initial metal nanomembrane. (c) Fabrication and immobilization of microsprings integrated on one step: Upper panel is a schematic diagram of rectangles patterned with an increasing misaligned angle in a step of  $10^\circ$ ; down panel is corresponding optical images of microsprings with a helical angle of  $83^\circ$  (1),  $73^\circ$  (2),  $63^\circ$  (3),  $53^\circ$  (4), and  $43^\circ$  (5).

calculated from the observation by optical microscopy. Panels III-VI of Fig. 3a display a series of the optical images of the grating-structured metallic microsprings with a helical angle of approximately  $18^\circ$ ,  $38^\circ$ ,  $56^\circ$ ,  $70^\circ$ , and the corresponding misaligned angle is  $72^\circ$ ,  $52^\circ$ ,  $35^\circ$ ,  $17^\circ$ , respectively, measured directly from the observed angles between the rectangles and the gratings. We also note several extreme situations: The rectangles rolled into multi-turns grating-structured microtubes (see panel I) with a tube length equal to the width of the initial rectangles when  $\beta = 90^\circ$ ; the grating-structured microscrews (see panel II) formed due to the overlap of adjacent turns when the value of  $\beta$  approaches  $90^\circ$ ; and the long microtubes (see panel VII) with a length equal to the length of the rectangles when  $\beta = 0^\circ$ . In addition, it is obvious that the grating structures on the walls of the 3D microstructures (*i.e.* microspring, microtube, and microscrew) were all parallel to their axial axis, suggesting that these structures self-aligned themselves to the orientation of the gratings, which is similar to the case demonstrated previously that the as-fabricated helices aligned themselves with the most close  $\langle 100 \rangle$  direction.<sup>16</sup> All these statistics were plotted and linearly fitted well with the solid line of  $\alpha + \beta = 90^\circ$  in Fig. 3b, which is another strong proof that the preferential rolling direction is perpendicular to the gratings. Additionally, from the synthetic standpoint of view, our approaches have the ability to synthesize both microsprings or helical structures with a helical angle varying from  $0^\circ$  to  $90^\circ$  and microtubes with an expected length to radius ratio in a more controllable and feasible manner. Moreover, to exploit the anisotropic

elasticity and further demonstrate the good control of helical angles, we have designed a lay-out composed of rectangles with misaligned angles increasing from  $7^\circ$  to  $47^\circ$  in a step of  $10^\circ$  relative to the gratings as schematically illustrated in upper panel of Fig. 3c. The counterparts after removing the sacrificial layer were presented in down panel of Fig. 3c, and the optical image evidently shows that the array of five grating-structured microsprings marked by '1' to '5' with a helical angle of  $83^\circ$ ,  $73^\circ$ ,  $63^\circ$ ,  $53^\circ$ , and  $43^\circ$ , respectively, have been fully released and anchored to the step with one end. It's alluring that all the microsprings coincidentally orientated parallel to each other and perpendicular to the preferential rolling direction, except for the deviating spring '5' owing to the external force from "the anchor" that resembles the kinked trench.<sup>35</sup>

### 3.4 Control of the diameter and the chirality

Other important properties like the diameter and the chirality of the grating-structured metallic microsprings can also be precisely tailored by this grating-directed rolling method. Two governing factors in the present experiment have been found to play a role in determining microspring diameter ( $D$ ): the film thickness ( $t$ ) and the grating period ( $\lambda$ ). Therefore, to study the dependence of  $D$  upon  $t$  and  $\lambda$ , systematic experiments were performed under two conditions: one at a constant grating period ( $\lambda = \sim 2.4 \mu\text{m}$ ) with varying film thickness; and the other at a constant film thickness ( $t = 40 \text{ nm}$ ) with varying grating periods (see Fig. S2, ESI†). The deposition rate was kept at  $4 \text{ \AA/s}$  for all samples. Collected optical images are summarized in Fig. 4a. It is noteworthy that the non-uniform cross-section of the grating-structured microsprings (see the inset of Fig. 4a) caused by the grating transfer can be ignored in this diameter calculation because the amplitude of gratings was too small compared to the total diameter. The dependences of the spring diameter on the film thickness and grating period are plotted in blue and red line, respectively, in Fig. 4a. It can be seen that the diameter of the microsprings increases almost linearly with the film thickness, consistent with the trend of rolled-up tubes and following well with the theoretical radius calculation.<sup>44</sup> To some extent, this similar rolling trend suggests that the approaches capable of tuning tube diameters can also be employed to acquire desired geometry of microsprings. On the other hand, the red curve suggests that the diameter of grating-structured microsprings also tends to increase with  $\lambda$ . The possible explanation is that the inner strain may be influenced at different level by varying  $\lambda$ . Furthermore, the chirality of the microsprings have been studied by orientating four strips labeled as 'I', 'II', 'III', and 'IV' respectively with a misaligned angle (relative to the gratings) of  $-45^\circ$ ,  $-25^\circ$ ,  $25^\circ$ , and  $45^\circ$  (see Fig. 4b). The SEM images in Fig. 4c imply that 'I' and 'II' formed right-handed microsprings with a helical angle of  $45^\circ$  and  $65^\circ$ , respectively, whereas 'III' and 'IV' formed left-handed

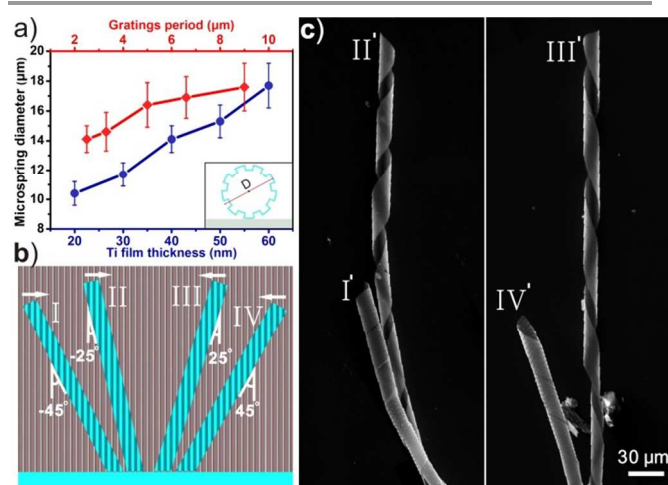


Fig. 4 (a) Microspring diameter as a function of Ti film thickness varying from 20 nm to 60 nm and a function of gratings period varying from 2.3  $\mu\text{m}$  to 9  $\mu\text{m}$ . Inset is the projection of the cross-section of the grating-structured microspring, illustrating the diameter measured from the outer walls. (b) Schematic diagrams illustrating the lay-out of four rectangles with a misaligned angle of  $-45^\circ$ ,  $-25^\circ$ ,  $25^\circ$ , and  $45^\circ$ , respectively, to control the chirality of the grating-structured microsprings. The arrows indicate the rectangles rolling direction. (c) Corresponding SEM images of the grating-structured microsprings with a helical angle of  $45^\circ$  (I'),  $65^\circ$  (II'),  $65^\circ$  (III'), and  $45^\circ$  (IV') respectively.

microsprings with a helical angle of  $65^\circ$  and  $45^\circ$ , respectively. Therefore, a preference to either right-handed or left-handed chirality can be simply determined by varying the orientation of rectangles. Overall, our approaches present a good control over the diameter and the chirality of the grating-structured metallic microsprings.

### 3.5 Properties of flowing rate sensing

As stated above, the advantages of utilizing grating structures to fabricate microsprings are two folds: creating a preferential rolling direction for strained nanomembranes and modifying the microsprings with grating structures. In the following, the performance of the grating-structured metallic microsprings in flow rate sensing<sup>31</sup> has been investigated. Since no additional assistant manipulation at micro-/nanoscale<sup>45</sup> was used, it is worth noting that the direction of the gratings before or after rolling should be parallel to the fluid flowing direction in the sensing system to guarantee that the as-fabricated microsprings are stretched by the dragging force exactly along the helical axis. As the fluid flowing rate increases, the microsprings extend longer in response, displaying a capability of detecting the fluid flowing rate as the smooth microsprings.<sup>31</sup> As presented in Fig. 5, the relationships between the fluid flowing rate and the elongation of four typical grating-structured microsprings (*i.e.* SP1, SP2, SP3, and SP4) are plotted using green squares, pink circulars, purple triangles, and blue stars, respectively. And the corresponding solid curves are from theoretical calculation engaging geometry parameters of the as-fabricated microsprings (see below and Table S2, ESI†). A good fit between the experiments and theory is

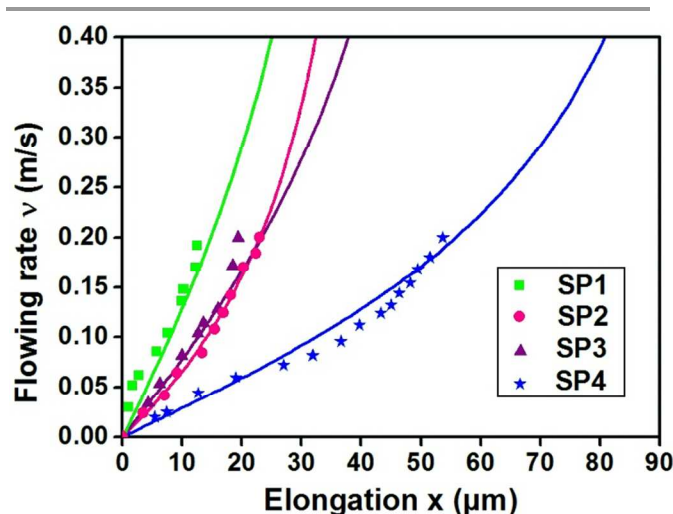


Fig. 5 Flowing rate ( $v$ ) versus elongation ( $x$ ) (solid curves) based on theoretical calculation (*i.e.* eqn (5)) fits the experimental data for SP1 ( $m = 2.0$ , plotted by green squares), SP2 ( $m = 2.7$ , plotted by pink circulars), SP3 ( $m = 4.0$ , plotted by purple triangles), and SP4 ( $m = 5.5$ , plotted by blue stars), respectively.

noticeable in Fig. 5.

To investigate the mechanical elasticity of the grating-structured microsprings in fluid, the periodic S-shaped cross-section of the grating-structured metallic nanomembranes (see Fig. S5(a), ESI†), which is distinguished from the general rectangular, square, or circular cross-section of previous micro/nano-springs or coils,<sup>7,31,45-47</sup> was carefully studied. Theoretically, the drag force of a smooth microspring  $F_{d-smooth}$ , counter-balanced by the “anchor force” from the fixed end, can be expressed by the following equation:<sup>31</sup>

$$F_{d-smooth} = \frac{2\mu lw}{\left[\ln\left(\frac{2L}{R}\right) - 0.72\right]R} v \quad (2)$$

where  $\mu$  represents the viscosity of the fluid (*i.e.* water);  $l$  and  $w$  are, respectively, the length and the width of the initial rectangles;  $L$  and  $R$  are, respectively, the length and the radius of the microspring;  $v$  is the real-time flowing rate. Note that the drag force  $F_d$  is proportional to the surface area, the applied drag force on the grating-structured microspring  $F_{d-structured}$  can therefore be derived from:

$$F_{d-structured} = F_{d-smooth} \cdot \frac{S_{structured}}{S_{smooth}} = \frac{2\mu lw}{\left[\ln\left(\frac{2L}{R}\right) - 0.72\right]R} v \cdot \left(1 + \frac{8\pi Rh}{\lambda^2}\right) \quad (3)$$

where  $S_{structured}$  and  $S_{smooth}$  are the total surface area of the grating-structured microspring and that of the smooth microspring, respectively;  $h$  and  $\lambda$  are the amplitude and the period of gratings, respectively. (The deduction of the relationship between  $S_{structured}$  and  $S_{smooth}$  is available in ESI†.) According to the classical elasticity theory, on the other hand, the spring constant  $K$  for a grating-structured microspring with  $m$  turns is given by:

$$\frac{1}{K} = \frac{6mp^2R^2}{Gl_0(1+\nu)\left[\left(1 + \frac{6h}{\lambda} - \frac{12h^2}{\lambda^2}\right)t^3 + \left(3h^2 + \frac{2h^3}{\lambda}\right)t\right]w \cos \beta} \quad (4)$$

where  $\nu$  and  $G$  are the Poisson's ratio and the shear modulus of the rolled material (*i.e.* Ti), respectively;  $l_0$  is the length of the initial nanomembrane before rolling into the grating-structured microspring. (Details on the deduction of eqn (4) are available in ESI†.) From eqn (4), one may note that the spring constant of this structured microspring changes greatly compared to that of the smooth microspring.<sup>31</sup> By assuming that the stretched microspring is under the state of equilibrium at an arbitrary flowing rate (*i.e.*  $F_{d-structured} = Kx$ ), the flowing rate  $v$  as a function of the elongation  $x$  is hence expressed as:

$$v = \frac{\pi G(1+\nu)\left[\left(1 + \frac{6h}{\lambda} - \frac{12h^2}{\lambda^2}\right)t^3 + \left(3h^2 + \frac{2h^3}{\lambda}\right)t\right] \frac{p_0}{\sqrt{4\pi^2 R_0^2 + p_0^2}}}{6\mu \left( \frac{4h \sqrt{4\pi^2 R_0^2 + p_0^2 - \left(\frac{mp_0+x}{m}\right)^2}}{\lambda^2} + 1 \right)} \cdot \frac{\ln \left[ \frac{4\pi(mp_0+x)}{\sqrt{4\pi^2 R_0^2 + p_0^2 - \left(\frac{mp_0+x}{m}\right)^2}} \right] - 0.72}{(mp_0+x)^2 \sqrt{4\pi^2 R_0^2 + p_0^2 - \left(\frac{mp_0+x}{m}\right)^2}} \cdot x \quad (5)$$

where  $R_0$  and  $p_0$  are the radius and the pitch of the microspring at relaxed state. (Detailed deduction of eqn (5) is also available in ESI†.)

This relation has been calculated by substituting numerical parameters, such as  $\mu = 0.001 \text{ Pa} \cdot \text{s}^{-1}$ ,  $G = 44 \text{ GPa}$ ,  $\nu = 0.33$  and other relative parameters described in Table S2 (see ESI†), and plotted using solid line in Fig. 5. The theoretical solid lines agree well with the respective experimental data in spite of a small deviation discussed in our previous investigation,<sup>31</sup> indicating that the theoretical model can predict the elastic behavior of the grating-structured metallic microsprings in fluid. Furthermore, the dependence of the flowing rate sensing properties upon the geometry of the gratings (*i.e.* the grating amplitude) was theoretically studied. Fig. S6 (see ESI†) reveals that the microsprings can achieve a longer elongation range with decreasing grating amplitude, demonstrating another route to well control the mechanic elasticity of the metallic

microsprings by adjusting the nanoimprint-tailored geometry of the gratings. Taking the potential applications into account, another advantage is appreciable that the rough morphology induced by grating structures is believed to show more striking optical properties such as the surface plasmon resonance (SPR) if the grating structures could scale down to an agreeable dimension. These optical properties may also facilitate the optical detection of the microspring elongation in the near future. Overall, the mechanical properties of the grating-structured metallic microsprings such as the elasticity can be affected and tuned by introducing grating structures, which are desirable for the potential application in bio-delivery and MEMS/NEMS devices.

## 15 Conclusions

In summary, we have demonstrated a controllable and rigorous technique to fabricate grating-structured metallic microsprings by rolling up strained rectangular nanomembranes deposited onto the nanoimprinted sacrificial layer in a fixed and structure-guided direction. The microsprings were found to be fabricated *via* misaligning the rectangular nanomembranes to the preferential rolling direction that derives from the grating induced anisotropic elastic energy state. This route also allows accessible tuning of the chirality and the diameter of the microsprings which shows a promising candidate for the synthesis of other complex three dimensional hierarchical micro-/nanostructures. The flow rate sensing property of the grating-structured microsprings was investigated and the sensing ability could be well tuned by the imprinting-controlled geometry of the gratings. The grating-structured micro-/nanostructures with a tailoring geometry and mechanical/optical properties may pave the way for their applications in MEMS/NEMS component and/or superlens.

## Acknowledgements

This work is supported by the Natural Science Foundation of China (Nos. 51322201 and 51102049), “Shu Guang” project by Shanghai Municipal Education Commission and Shanghai Education Development Foundation, Project Based Personnel Exchange Program with CSC and DAAD, Specialized Research Fund for the Doctoral Program of Higher Education (No. 20120071110025), the National Basic Research Program of China (Grant No. 2011BAF06B01) and Science and Technology Commission of Shanghai Municipality (No. 12520706300). RL thanks the support from the National High Technology Program (2011AA100706-2) and the National Science Foundation of China (61171010). Part of the experimental work has been carried out in Fudan Nanofabrication Laboratory.

## Notes and references

- 51 <sup>a</sup> State Key Lab of ASIC and System, Fudan University, Shanghai 200433, People's Republic of China. E-mail: rliu@fudan.edu.cn  
<sup>b</sup> Department of Materials Science, Fudan University, Shanghai 200433, People's Republic of China. E-mail: yfm@fudan.edu.cn  
† Electronic Supplementary Information (ESI) available: See DOI:
- 57 1 V. Ya. Prinz, V. A. Seleznev, A. K. Gutakovskiy, A. V. Chehovskiy, V. V. Preobrazhenskii, M. A. Putyato and T. A. Gavrilova, *Phys. E.*, 2000, **6**, 828.
- 60 2 W. Han, S. Fan, Q. Li and Y. Hu, *Science*, 1997, **277**, 1287.  
3 P. X. Gao, Y. Ding, W. Mai, W. L. Hughes, C. S. Lao and Z. L. Wang, *Science*, 2005, **309**, 1700.
- 63 4 J. Zhu, Z. Yu, G. F. Burkhard, C.-M. Hsu, S. T. Connor, Y. Xu, Q. Wang, M. McGehee, S. Fan and Y. Cui, *Nano Lett.*, 2008, **9**, 279.
- 66 5 Z. Fan, H. Razavi, J.-W. Do, A. Moriwaki, O. Ergen, Y.-L. Chueh, P. W. Leu, J. C. Ho, T. Takahashi, L. A. Reichertz, S. Neale, K. Yu, M. Wu, J. W. Ager and A. Javey, *Nat. Mater.*, 2009, **8**, 648.
- 69 6 S. Schwaiger, M. Broll, A. Krohn, A. Stemmann, C. Heyn, Y. Stark, D. Stickler, D. Heitmann and S. Mendach, *Phys. Rev. Lett.*, 2009, **102**, 163903.
- 72 7 X. Chen, S. Zhang, D. A. Dikin, W. Ding, R. S. Ruoff, L. Pan and Y. Nakayama, *Nano Lett.*, 2003, **3**, 1299.
- 75 8 J. T. Hu, O. Y. Min, P. D. Yang and C. M. Lieber, *Nature*, 1999, **399**, 48.  
9 K. B. Zhou, X. Wang, X. M. Sun, Q. Peng and Y. D. Li, *J. Catal.*, 2005, **229**, 206.
- 78 10 E. Garnett and P. Yang, *Nano Lett.*, 2010, **10**, 1082.  
11 R. A. Tripp, R. A. Dluhy and Y. Zhao, *Nano Today*, 2008, **3**, 31.
- 81 12 Z. L. Wang, *Appl. Phys. A: Solid Surf.*, 2007, **88**, 7.  
13 D. M. Sun, M. Y. Timmermans, Y. Tian, A. G. Nasibulin, E. I. Kauppinen, S. Kishimoto, T. Mizutani and Y. Ohno, *Nat. Nanotechnol.*, 2011, **6**, 156.
- 84 14 K. W. Park, Y. E. Sung, S. Han, Y. Yun and T. Hyeon, *J. Phys. Chem. B*, 2004, **108**, 939.
- 87 15 P. X. Gao and Z. L. Wang, *Small*, 2005, **1**, 945.  
16 D. J. Bell, L. Dong, B. J. Nelson, M. Golling, L. Zhang and D. Grützmacher, *Nano Lett.*, 2006, **6**, 725.
- 90 17 Y.-P. Zhao, D.-X. Ye, G.-C. Wang and T.-M. Lu, *Proc. SPIE*, 2003, **5219**, 59.  
18 Dong, L. Zhang, D. J. Bell, D. Grützmacher and B. J. Nelson, *J. Phys. Conf. Ser.*, 2007, **61**, 257.
- 93 19 S. Tottori, L. Zhang, F. Qiu, K. K. Krawczyk, A. Franco-Obregón and B. J. Nelson, *Adv. Mater.*, 2012, **24**, 811.
- 96 20 L. Zhang, J. J. Abbott, L. X. Dong, B. E. Kratochvil, D. Bell and B. J. Nelson, *Appl. Phys. Lett.*, 2009, **94**, 064107.  
21 S. Motojima, Y. Noda, S. Hoshiya and Y. Hishikawa, *J. Appl. Phys.*, 2003, **94**, 2325.
- 99 22 S. V. Kesapragada, P. Victor, O. Nalamasu and D. Gall, *Nano Lett.*, 2006, **6**, 854.
- 102 23 E. D. Sone, E. R. Zubarev and S. I. Stupp, *Angew. Chem., Int. Ed.*, 2002, **41**, 1705.  
24 L. Liu, S. H. Yoo, S. A. Lee and S. Park, *Nano Lett.*, 2011, **11**, 3979.

- 25 J. X. Li, S. Sattayasamitsathit, R. F. Dong, W. Gao, R. Tam, X. M. Feng, S. Ai, and J. Wang, *Nanoscale*, 2014.
- 3 26 J. K. Gansel, M. Thiel, M. S. Rill, M. Decker, K. Bade, V. Saile, G. von Freymann, S. Linden and M. Wegener, *Science*, 2009, **325**, 1513.
- 6 27 G. S. Huang and Y. F. Mei, *Adv. Mater.*, 2012, **24**, 2517.
- 28 L. Zhang, E. Deckhardt, A. Weber, C. Schonenberger and D. Grutzmacher, *Nanotechnology*, 2005, **16**, 655.
- 9 29 P. Froeter, X. Yu, W. Huang, F. Du, M. Y. Li, I. S. Chun, S. H. Kim, K. J. Hsia, J. A. Rogers, and X. I. Li, *Nanotechnology*, 2013, **24**, 475301.
- 12 30 M. Huang, C. Boone, M. M. Roberts, D. E. Savage, M. G. Lagally, N. Shaji, H. Qin, R. Blick, J. A. Nairn and F. Liu, *Adv. Mater.*, 2005, **17**, 2860.
- 15 31 W. M. Li, G. S. Huang, J. Wang, Y. Yu, X. J. Wu, X. G. Cui and Y. F. Mei, *Lab Chip*, 2012, **12**, 2322.
- 32 W. M. Li, G. S. Huang, H. Yan, J. Wang, Y. Yu, X. H. Hu, X. J. Wu and Y. F. Mei, *Soft Matter*, 2012, **8**, 7103.
- 18 33 A. B. Vorob'ev and V. Y. Prinz, *Semicond. Sci. Technol.*, 2002, **17**, 614.
- 21 34 T. Kipp, H. Welsch, C. Strelow, C. Heyn and D. Heitmann, *Phys. Rev. Lett.*, 2006, **96**, 077403.
- 35 Ch. Deneke and O. G. Schmidt, *Appl. Phys. Lett.*, 2004, **85**, 2914.
- 24 36 Y. F. Mei, G. Huang, A. A. Solovev, E. Bermudez Urena, I. Mönch, F. Ding, T. Reindl, R. K. F. Fu, P. K. Chu and O. G. Schmidt, *Adv. Mater.*, 2008, **20**, 4085.
- 27 37 I. S. Chun, A. Challa, B. Derickson, K. J. Hsia and X. Li, *Nano Lett.*, 2010, **10**, 3927.
- 38 S. Alben, B. Balakrishnan and E. Smela, *Nano Lett.*, 2011, **11**, 2280.
- 30 39 P. Cendula, S. Kiravittaya, I. Mönch, J. Schumann and O. G. Schmidt, *Nano Lett.*, 2011, **11**, 236.
- 33 40 Z.-C. Xu, B. Dong, B.-R. Lu, Y. Chen, E. Huq, X.-P. Qu and R. Liu, *Microelectron. Eng.*, 2011, **88**, 2647.
- 41 P. Carlberg, M. Graczyk, E.-L. Sarwe, I. Maximov, M. Beck and L. Montelius, *Microelectron. Eng.*, 2003, **67-68**, 203.
- 36 42 K. Pfeiffer, F. Reuther, M. Fink, G. Gruetzner, P. Carlberg, I. Maximov, L. Montelius, J. Seekamp, S. Zankovych, C. M. Sotomayor-Torres, H. Schulz and H. C. Scheer, *Microelectron. Eng.*, 2003, **67-68**, 266.
- 39 43 J. X. Li, J. Zhang, W. Gao, G. S. Huang, Z. Di, R. Liu, J. Wang and Y. F. Mei, *Adv. Mater.*, 2013, **25**, 3715.
- 42 44 R. Songmuang, C. Deneke and O. G. Schmidt, *Appl. Phys. Lett.*, 2006, **89**, 223109.
- 45 45 P. X. Gao, W. Mai and Z. L. Wang, *Nano Lett.*, 2006, **6**, 2536.
- 46 L. Dai, L. Zhang, L. X. Dong, W. Z. Shen, X. B. Zhang, Z. Z. Ye and B. J. Nelson, *Nanoscale*, 2011, **3**, 4301.
- 48 47 H. Bi, K. C. Kou, K. Ostrikov, J. Q. Zhang and Z. C. Wang, *J. Appl. Phys.*, 2009, **106**, 023520.